JOURNAL OF MATERIALS SCIENCE: MATERIALS IN MEDICINE 1 (1990) 211–218

The effect of beryllium on the corrosion resistance of nickel–chromium dental alloys

TZYY-PING CHENG*, WEN-TA TSAI*, JIIN-HUEY CHERN LIN‡, JU-TUNG LEE*
*Department of Materials Engineering, National Cheng Kung University, Tainan, Taiwan, China
‡Department of Biological Materials, Northwestern University, Chicago, Illinois, USA

Base-metal alloys of the nickel–chromium system are widely applied in fixed prosthodontics. The principal purpose of the addition of beryllium is to increase the fluidity of the Ni–Cr alloy during melting and increase the castability. In this study the effects of beryllium addition, by weight percentages of 0.5, 1.0 and 2.0, respectively, on the microstructure and corrosion resistance of seven Ni–Cr-based and NP2-based dental alloys were examined in Ringer's solution at 37° C. The experimental results indicate that addition of beryllium has a very significant effect on lowering the pitting potentials, open-circuit potentials, passive-film resistances and, on the contrary, increasing the passive-film capacitances. The presence of beryllium greatly reduces the thickness of the passive film and makes the corrosion resistance worse. This effect is more pronounced for NP2-based dental alloys. Examination of the corroded surfaces reveals that it is the Ni–Be eutectic phase being preferentially attacked.

1. Introduction

Base-metal alloys of the Ni–Cr system currently account for a sizeable portion of the fixed prosthesis alloy market [1]. The low price of these alloys is one of their major attractions. Applications of these Ni–Cr alloys in fixed prosthodontics are to use them as a base alloy for porcelain application such as Maryland bridge or framework for a partial denture. However, the uses of such Ni–Cr base alloys for fixed prosthodontics are limited because questions exist about the nickel sensitivity and the overall performance of such alloys [1].

The binary phase diagram for the Ni–Cr system shows extensive solid solubility of chromium in nickel [2]. Chromium provides corrosion resistance and some solution hardening, and other additives are used to provide more solid solution hardening or precipitate formation. The purposes of the addition of beryllium to Ni–Cr dental alloys are threefold; first, it can effectively lower the melting point and make the casting process much easier [2]. Secondly, it can increase the fluidity and castability of the Ni–Cr alloys [3]. Thirdly, the addition of beryllium is believed to decrease slightly the corrosion resistance of the alloys [4, 5], and this makes the etching process of Maryland bridge easier. Therefore, commercially available Ni–Cr alloys such as Ultratek (Ultratek International Inc., Concord, California, USA), Litecast B (Williams Gold and Refining Co., Buffalo, New York, USA), Gemini II (Kerr Mfg. Co., Romulus, Michigan, USA), etc., have been alloyed with beryllium. However, an unfavourable drawback exists: the release of the dermatotoxic nickel and the carcinogenic beryllium ions when the Ni–Cr–Be alloy corrodes [5].

Passivation of the metal surface is a very effective way to decrease the corrosion rate, and the tendency of passivation is strongly dependent on the type and the amount of alloying elements. Chromium, in particular, is very well known as the major constituent of the passive film on the surface of Ni–Cr alloys and provides a beneficial effect on the reduction of the corrosion rate. Other alloying elements can also be incorporated into the structure of the passive film and can cause beneficial or detrimental changes of electrochemical characteristics of this passive film. For example, molybdenum and manganese improve the pitting resistance [6]. Conversely, the alloying element beryllium provides a detrimental effect on the corrosion resistance, lowering the pitting potentials significantly, as a previous study indicated [5]. The specific role that beryllium plays in the passive film properties is, however, not very clear when beryllium-containing dental alloys are installed clinically. The method of polarization profiles which was utilized in [5] can reveal the pitting potentials as a function of the beryllium content, which could result in breakdown of the passive film at comparatively low potentials. However, the "real" electrochemical characteristics of the passive film in freely corroding conditions have not yet been evaluated, since the potential applied by the traditional d.c. polarization techniques is generally too high, and deviates significantly from the open-circuit potential (OCP) and so does not show the real situation that the dental alloys meet. Electrochemical impedance spectroscopy offers the possibility of evaluating the true surface properties of beryllium-containing dental alloys at OCPs. In this investigation the effect of beryllium on the electrochemical parameters of

0957–4530/90 $03.00 + .12

the passive film is of great concern and is evaluated semiquantitatively.

2. Data analysis

Electrochemical impedance (a.c. impedance) measurements are finding increasing applications in corrosion research, due to a number of advantages that they have over the traditional d.c. techniques, such as: (1) the application of a small oscillatory voltage around the OCP (about 10 mV) which does not disturb the electrode properties to be measured and (2) both the polarization resistance and the double-layer capacitance can be obtained in one measurement [7, 8]. It was also reported that the electrochemical impedance technique could be used to estimate the corrosion resistance of an alloy with an extremely low corrosion rate [9–11].

The electrical analogue of the corroding metal surface can be demonstrated and represented by a network consisting of resistors and capacitors – the equivalent circuit. Evaluation of the components of the equivalent circuit provides a characteristic measurement of the surface properties and an estimate of the corrosion resistance. The electrochemical reaction at the metal–solution interface is generally assumed to be very simple in nature and could be represented by the equivalent circuit shown in Fig. 1a. This circuit consists of the solution resistance R_0 between the surface and the reference electrode. The charge transfer resistance R_{ct} is in parallel with the double-layer capacitance C_{dl}. Another RC circuit is in series with R_{ct} and C_{dl}, containing the passive-film resistance R_{pf} and the passive-film capacitance C_{pf}. If the passive-film impedances (R_{pf} and C_{pf}) dominate the electrochemical reaction, then Fig. 1a can be simplified and illustrated as Fig. 1b. Furthermore, if the electrode process takes into account the diffusion of charged species, another component known as the Warburg impedance will appear in the equivalent circuit. The surface interaction of the passive film with the aggressive environment can be analysed and represented by this simple model.

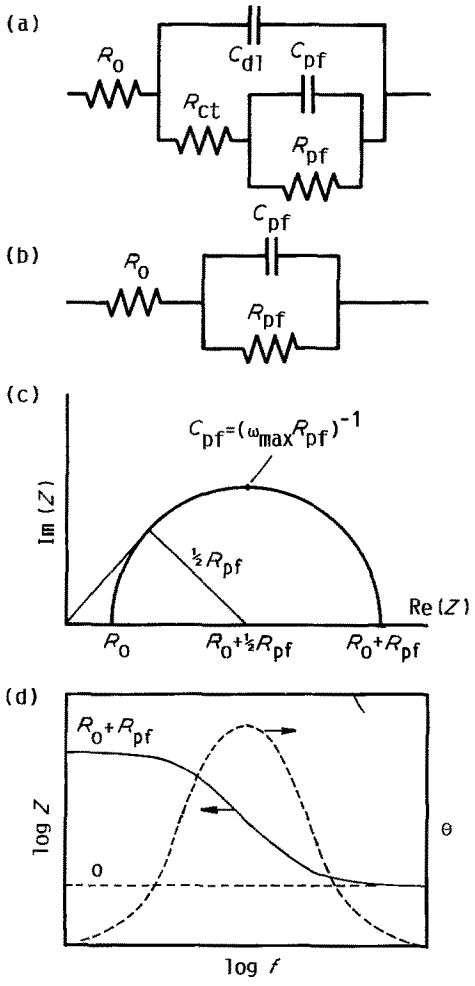

Figure 1 (a) Equivalent circuit of the surface property of a passive metal and (b) its simplified model. Impedance data can be displayed in the form of a Nyquist plot (c) or a Bode plot (d).

The measured impedance data can be displayed in the form of a Bode plot and/or a Nyquist plot, as shown schematically in Figs 1c and 1d, respectively. The Bode plot shows the frequency dependence of the absolute magnitudes of the impedance modulus and the phase angle. In the Bode diagram the measured impedance modulus will approach the value of the solution resistance R_0 at the high-frequency end, and will approach the sum of the solution resistance, the charge transfer resistance and the passive-film resistance ($R_0 + R_{ct} + R_{pf}$) at the low-frequency end. At these two frequency extremes the phase angle is found to be near 0° and this shows that the electrode properties can be represented by an ideal resistor whose response to an a.c. signal is nearly independent of the frequency. If the impedance data are displayed by the complex variables and separated into real and imaginary parts, a semicircle is plotted in this complex plane plot which is called a Nyquist plot. A detailed analysis of such an equivalent circuit is outside the scope of this paper and is described elsewhere [7, 8].

3. Experimental procedures

3.1. Preparation of alloys and solution

Two groups of Ni–Cr alloys were used, namely the Ni–15% Cr alloy and Microbond NP2 alloy (Howmedica Inc., Chicago, Illinois, USA) whose major chemical composition is Ni–13% Cr–7% Mo–7.5% Fe, Si, Mn. All of these Ni–Cr alloys that were supplied by the manufacturer of dental alloys (Austenal Laboratories) were induction cast and alloyed with 0.5 wt%, 1.0 wt%, and 2.0 wt% beryllium. The chemical compositions are listed in Table I and these alloys were designated alloys A to G.

While conducting electrochemical tests, all specimens were wrapped with Teflon tape, only one face of the specimen being exposed to the solution. In order not to provoke crevice corrosion in the gap between

TABLE I Chemical compositions of the Ni–Cr alloys

Alloy	Chemical composition
A	Ni–15Cr
B	Ni–15Cr–0.5Be
C	Ni–15Cr–1.0Be
D	Ni–15Cr–2.0Be
E	NP2–0.5Be
F	NP2–1.0Be
G	NP2–2.0Be

the Teflon tape and the specimens, all of these gaps were well sealed by a quick-setting cyanoacrylate adhesive. The exposed surfaces of surface area about 0.34 cm^2 were polished through the standard metallurgical polishing procedure to 1 μm alumina powder before conducting the electrochemical test. Ringer's solution was selected as the testing environment and was prepared from reagent-grade chemicals and distilled water. It contained 9.0 g NaCl, 0.42 g KCl, 0.24 g $CaCl_2$ and 0.2 g $NaHCO_3$ per litre distilled water. The temperature of the testing solution was controlled at 37° C.

3.2. Electrochemical evaluation

In order to compare the effect of beryllium addition to the Ni–Cr alloys, the electrochemical behaviour of these alloys was assessed by tracing the cyclic potentiodynamic polarization curves for each alloy in de-aerated solution which is very close to the corrosive environment encountered in the crevice. The mechanistic parameters of the surface properties were also determined according to the electrochemical impedance method described by Mansfeld [7]. The variations of the OCPs of each alloy with time were monitored by high input-impedance electrometers in de-aerated and aerated Ringer's solution. The former was employed to simulate the corrosion environment in the crevice, and the latter to simulate the oral environment and to take into account the influence of dissolved oxygen.

Potentiodynamic polarization tests at a scan rate of 1 mV sec^{-1} were conducted to evaluate the characteristic electrochemical parameters, namely the corrosion potential E_{corr}, the critical potential E_{cr} and the critical current density i_{cr} for the active-to-passive transition, the pitting potential E_p, the pitting protection potential E_{pp} and the passive current density i_p, of the Ni–Cr alloys. All of these potentials are reported with respect to the saturated calomel electrode (SCE). The specimens were first cathodically polarized at − 1000 mV(SCE) for 5 min to clean the metal surfaces. Then the potential of the specimen was scanned from − 1000 mV(SCE) towards the more positive direction until the vertex potential where its corresponding current density was 5000 $\mu A\,cm^{-2}$, as recommended by ASTM G61 standard practice. The pitting potential was found and taken as the initiation potential of pitting corrosion. The potential was then scanned backwards again to locate the pitting protection potential, which was defined as the intercept of the forward and the reverse scan curves. After the polarization test, the corrosion morphology of the specimens was observed by using optical and electron microscopy.

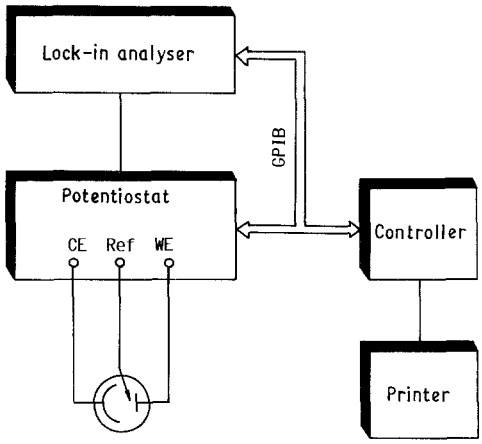

Figure 2 Schematic diagram of the instrumental arrangement.

Measurements by electrochemical impedance spectroscopy in aerated and de-aerated Ringer's solution were carried out and analysed by a PAR (Princeton Applied Research Co.) model 273 potentiostat and model 5208 lock-in analyser. The set-up of the analysing instruments is shown in Fig. 2. These impedance measurements were made by applying a small amplitude perturbation, with amplitude 10 mV in a sinusoidal form, and by scanning the modulus of impedance and the phase shift over the frequency range from 100 kHz to 1 mHz. The d.c. potential of each specimen was controlled at the respective OCP. Before each test every specimen was cathodically polarized at − 1000 mV as described for the measurement of the polarization curve. After the OCP reached the steady state, the monitoring of impedance spectroscopy was initiated. A platinum screen was used as the counter-electrode to surround the working electrode.

4. Results and discussion

4.1. Polarization behaviour

Cyclic potentiodynamic polarization curves for Ni–Cr dental alloys in de-aerated Ringer's solution are shown in Figs 3 and 4. The characteristic potentials and current densities obtained from these polarization curves are all listed in Table II. Basically, the corrosion potentials and critical potentials for the active-to-passive transition of Ni–15Cr-based alloys (alloys A to D) do not follow the trend of increasing beryllium content and show no particular order at all. On the other hand, the pitting potentials, the pitting protection potentials and the passivation ranges ($E_p - E_{cr}$) are strongly dependent on the weight

TABLE II Electrochemical parameters of polarization curves in de-aerated Ringer's solution at 38° C

Alloy	E_{corr} (mV)	E_{cr} (mV)	E_p (mV)	E_{pp} (mV)	i_{cr} ($\mu A\,cm^{-2}$)	i_p ($\mu A\,cm^{-2}$)	$E_p - E_{cr}$ (mV)
A	−808	−747	−79	−183	13.0	6.8	668
B	−784	−747	−115	−280	7.6	5.4	632
C	−808	−752	−143	−300	10.5	5.1	609
D	−768	−723	−135	−324	4.8	3.6	588
E	−912	−852	169	−244	27.0	2.9	1021
F	−856	−812	−3	−315	9.5	4.0	809
G	−868	−828	−110	−320	9.2	3.2	718

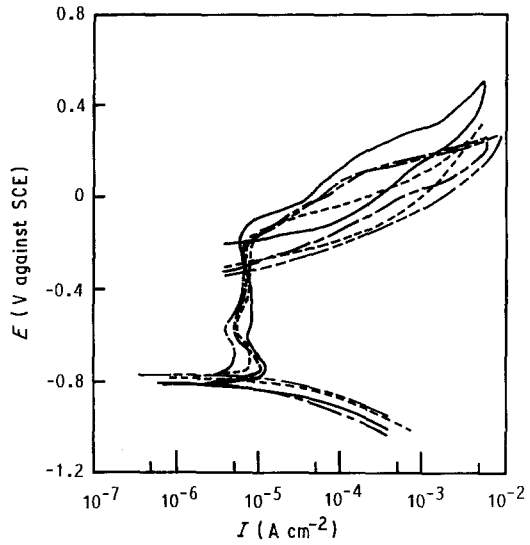

Figure 3 Potentiodynamic polarization curves of Ni–15Cr-based alloys (alloys A to D) in de-aerated Ringer's solution with a scan rate of 1 mV (sec^{-1} at 37° C. (——) Alloy A, (– – –) alloy B, (– – –) alloy C and (– – – –) alloy D.

percentages of beryllium added, as shown in Fig. 5. The pitting protection potentials shift to more-negative values as the amount of beryllium is increased. As little as 0.5 wt % beryllium addition could lower the pitting protection potental greatly. The results suggest that beryllium has a detrimental effect on the repassivation kinetics. The change in the pitting protection potentials shows a very similar tendency to the change in the pitting potentials. The passivation ranges, the potential regions between pitting potentials and critical potentials have been reduced much less due to the addition of beryllium than those of NP2-based alloys (Fig. 5).

Compared with the Ni–15Cr-based dental alloys, the variations of the corresponding polarization behaviour with the amount of beryllium obtained for NP2-based alloys (alloys E to G) demonstrate a very similar tendency in Ringer's solution. The corrosion

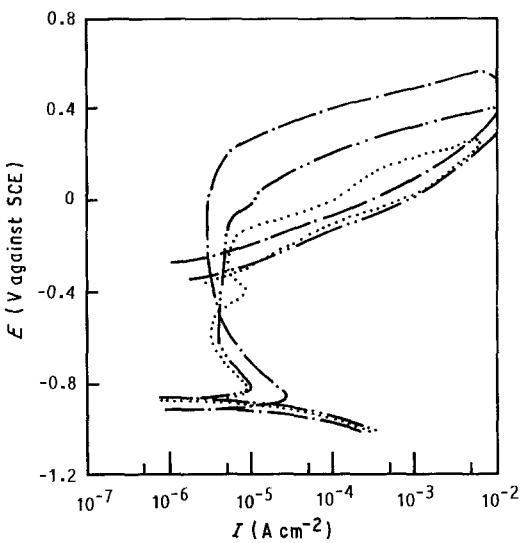

Figure 4 Potentiodynamic polarization curves of NP2-based alloys (alloys E to G) in de-aerated Ringer's solution with a scan rate of 1 mV sec^{-1} at 37° C. (–·–·–) Alloy E, (—··—) alloy F and (···) alloy G.

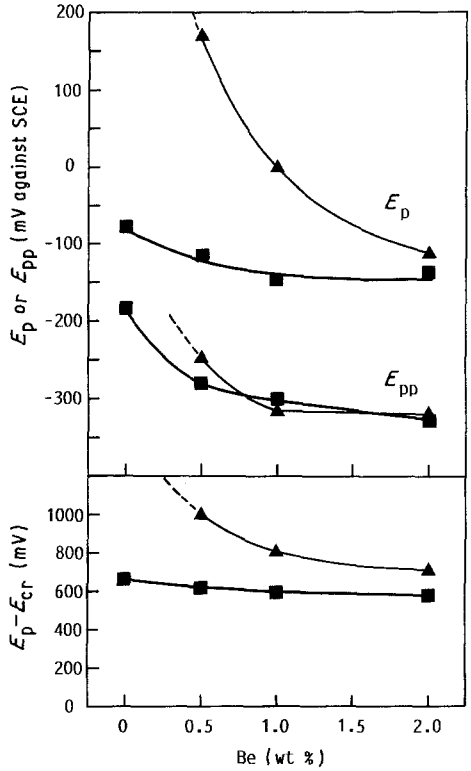

Figure 5 Effect of beryllium content on the lowering of the pitting protection potentials and the passivation ranges. (▲) NP2-xBe and (■) Ni–15Cr–xBe.

potentials and critical potentials of NP2-based alloys are more negative than those of Ni–15Cr-based alloys. Pitting potentials, on the contrary, are much nobler, implying that the initiation of corrosion pits in these NP2-based alloys is more energetically barricaded. It was reported [6] that not only is the presence of chromium needed to increase the ability to passivate such alloys, in the Ni–Cr alloy a small amount of alloying elements such as molybdenum and gallium is also necessary to provide additional protection against pitting. The difference between the electrochemical properties of the Ni–15Cr-based alloys and the NP2-based alloys is due mainly to the high molybdenum and gallium contents of the latter alloys. The addition of beryllium has a significant effect on lowering the pitting potentials. The extent of the reduction of the pitting potential is much more significant for NP2-based alloys than for Ni–15Cr-based alloys (see Table II), but they still have nobler pitting potentials because of the existence of other alloying elements such as molybdenum and gallium.

Previous examination of polarization profiles [5] revealed that the pitting potential of NP2 alloy is lowered by about 100 mV in aerated conditions when the beryllium content is increased from 0.5 to 2 wt %. However, a more pronounced effect (with an about 280 mV decrease in the pitting potential in the same range of beryllium content) of beryllium addition is observed in de-aerated Ringer's solution. It is believed that localized corrosion is more likely to occur in the oxygen-deficient environment while the effect of the differential aeration cell is working. The oxidizing power of the oxygen-deficient Ringer's solution in the crevice is decreased and the beryllium-containing Ni–Cr alloys passivate themselves less

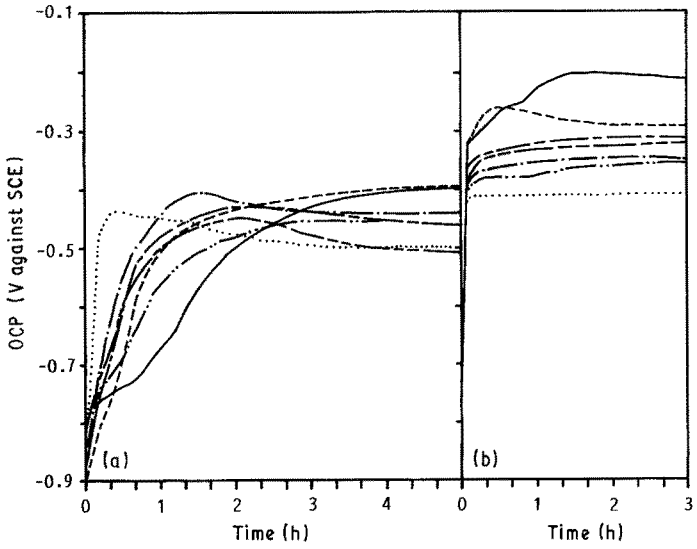

Figure 6 Variations of OCPs plotted against time in (a) de-aerated and (b) aerated Ringer's solution at 37° C. Key as in Figs 4 and 5.

readily under such circumstances. Therefore, the beryllium-containing Ni–Cr alloys are prone to localized corrosion, especially in the crevice area between dental alloys and other tissues if installed clinically. Although NP2-based alloys exhibit much more-positive pitting potentials, their pitting protection potentials are almost the same as those of the Ni–15Cr-based alloys at beryllium contents exceeding 0.5 wt % (see Table II and Fig. 5). The reduction of the passivation range is also more evident for NP2-based alloys. This phenomenon shows that the addition of beryllium to NP2 alloy has a more detrimental effect on the reduction of the corrosion resistance, even though the amount of beryllium addition is as low as 0.5 wt %.

The passive-current densities are in the range of 3 to 7 μA cm^{-2}, but without any particular order. Sutow *et al.* [4], however, reported that the current densities of beryllium-containing alloys in a crevice are higher than those for alloys without beryllium. The discrepancy probably results from the difference between the corrosive environments, i.e. it depends on the metal surface exposed to either neutral electrolyte or acidified crevice solution.

The variation of the OCP of each alloy in either de-aerated or aerated Ringer's solution was monitored and is shown in Fig. 6. The time required for the OCPs to reach the steady state and to passivate the metal surface is considered as an indicator of the passivating power of dental alloys. The results show that the content of dissolved oxygen in Ringer's solution and the alloy type are two major controlling factors. The OCPs in aerated Ringer's solution could approach the steady-state values within a very short time, implying that the dissolved oxygen could help to passivate the dental alloys. The steady-state OCPs are lowered as the beryllium content increases, and the OCPs of NP2-based alloys are more negative than those of Ni–15Cr-based alloys. This phenomenon is similar to that found in polarization measurements as described above. In de-aerated Ringer's solution the trend of variations of OCPs is very similar to that in the aerated solution, but the alloys require a longer time to reach the steady state at less-positive potentials.

4.2. Impedance spectroscopy

A.c. impedance spectroscopy of de-aerated Ringer's solution, displayed in the form of Bode plots, are shown in Figs 7 and 8. In aerated solution impedance spectroscopy (not shown) shows a very similar trend of impedance changes but with different values of the electrochemical parameters. The d.c. potential of each specimen was controlled at the steady-state OCP, found to locate within the passive region. In this study impedance spectroscopy of these Ni–Cr alloys indicates that the surface interaction of these alloys is similar and could be characterized by the simple equivalent circuit model shown in Fig. 1. Only one maximum value of the phase lag is observed for each alloy. This result indicates that the impedance of the passive film is much greater and overshadows that of the double-layer equivalent *RC* circuit. Therefore, the equivalent circuit with two *RC* circuits in series can be simplified to eliminate the double-layer *RC* circuit, as shown in Fig. 1b, since the influence of the double-layer components is relatively small. Accordingly, the

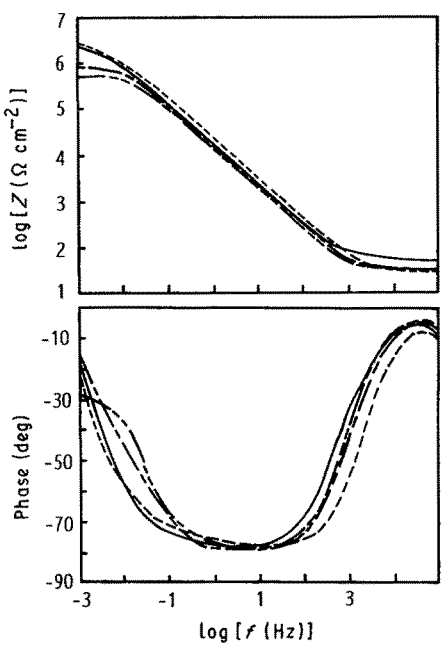

Figure 7 A.c. impedance spectroscopy in the form of Bode plots for Ni–15Cr-based alloys (alloys A to D) in de-aerated Ringer's solution. Key as in Fig. 3.

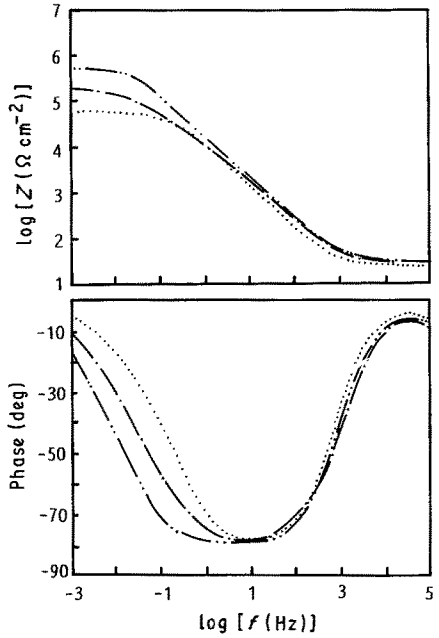

Figure 8 A.c. impedance spectroscopy in the form of Bode plots for NP2-based alloys (alloys E to G) in de-aerated Ringer's solution. Key as in Fig. 4.

respective impedance moduli of the equivalent electric component could be calculated easily from the Bode plot, and these are listed in Table III. The parallel capacitance, i.e. the passive-film capacitance, of the equivalent circuit is calculated from w_{max}, according to [7]

$$C_{pf} = 1/\omega_{max} R_{pf} \quad (1)$$

where ω_{max} is the corresponding angular frequency of the impedance at the apex of the semicircle of the Nyquist plot.

The passive-film resistances derived from impedance spectroscopy in both de-aerated and aerated Ringer's solution show that they decrease as the weight percentage of beryllium increases. The extent of the decrease is more obvious fo NP2-based alloys. The results are in good agreement with those obtained in polarization tests. On the other hand, the passive-film resistances derived in de-aerated solution are much greater than those derived in aerated solution. This may be attributed to the differences in the potentials (OCPs) and in the dissolved oxygen contents of Ringer's solution in which a.c. impedance spectroscopy was conducted. In de-aerated conditions the OCPs are more negative than their counterparts in aerated solution and are at least 125 mV more negative than the pitting protection potentials. The OCPs in aerated solution are on the verge of the pitting protection potentials. Therefore, the film dissolution and breakdown process is in competition with the film formation and thickening process. Consequently, the passive film which is formed with a compromise of the film dissolution process in aerated Ringer's solution is less compact and thinner than the passive film formed in de-aerated solution at more-negative potentials. Therefore, the passive-film resistance is reduced.

The passive-film capacitances were also calculated. However, the centre of the semicircular Nyquist plots in the complex plane were found to fall below the real axis. This type of deviation had been commonly reported in the literature [10, 12]. One explanation for this effect is that the uneven current distribution caused by a porous surface layer or a highly roughened surface can facilitate this depression [12]. The occurrence of the depressed semicircle could cause an error in the calculation by applying Equation 1 directly. The parallel capacitances listed in Table III are, thus, estimated values calculated by Equation 1. It is frequently assumed that the reciprocal value of the passive-film capacitance is linearly proportional to the thickness of the passive film on the metal surface, regardless of other influential factors [13]. Hence, the passive-film thickness of alloy A (with no beryllium addition) is greatest for the lowest capacitance and highest resistance values. The smaller impedance values (i.e. smaller passive-film resistances and greater passive-film capacitances) of the beryllium-contaning Ni–Cr alloys show that their passive-film thickness could be diminished greatly as a result of beryllium addition. Therefore, the presence of beryllium in the Ni–Cr alloy could reduce the corrosion resistance greatly and make the passive-film thickening process more difficult. The susceptibility to localized corrosion is also greatly increased. Furthermore, the charged species would penetrate through the surface film with little difficulty. Therefore, all of the Ni–Cr alloys containing beryllium, having greater passive-film capacitances and smaller passive-film resistances, show inferior corrosion resistance to alloy A due to thinner passive film and easier penetration of aggressive and other charged species.

4.3. Microstructure analysis

Analysis of the cast microstructure of dental alloys

TABLE III Passive-film resistances and passive-film capacitances calculated from impedance spectroscopy in aerated and de-aerated Ringer's solution at 37° C

Alloy	Aerated			De-aerated		
	OCP (mV)	R_{pf} (kΩ cm^{-2})	C_{pf} (μF cm^{-2})	OCP (mV)	R_{pf} (kΩ cm^{-2})	C_{pf} (μF cm^{-2})
A	−214	370	9	−376	2020	NA
B	−277	269	28	−418	1240	NA
C	−313	63	37	−461	879	12
D	−316	55	26	−449	508	29
E	−342	867	37	−407	1030	9
F	−363	140	46	−454	407	12
G	−409	24	59	−497	59	57

NA, not available in the test frequency range, due to its large time constant.

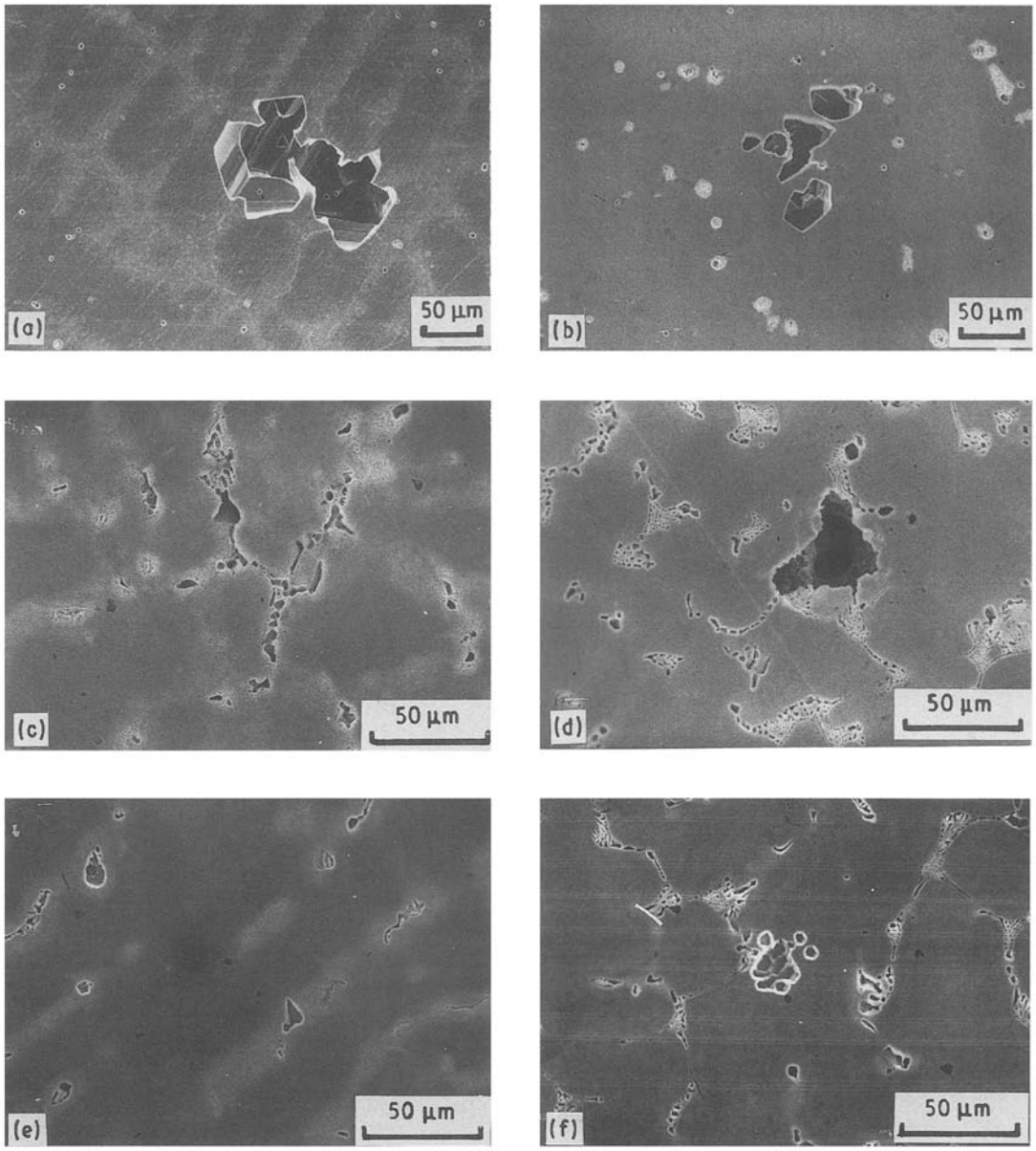

Figure 9 Scanning electron micrographs showing the pitting morphology on the surface of polished Ni–Cr alloys (alloys A to G) after anodic polarization to a current density of 5000 $\mu A\,cm^{-2}$.

shows that dendrite arms of composition Ni–Cr have been developed when solidifying from the melt. The Ni–Be eutectic phase is also formed sequentially within the interdendritic arm spacing because of its lower melting point. From previous research [5] we know that the volume fraction of Ni–Be eutectic phase increases with increasing beryllium addition. Examination of the corroded surfaces of dental alloys after immersion tests in Ringer's solution, compared with the chemically etched microstructure, reveals that it is this Ni–Be eutectic phase being preferentially attacked. This indicates that the corrosion resistance is lowered as the beryllium content increases.

The corroded surface morphology of the polished surfaces after polarization measurements are shown in Fig. 9. The larger pits on the surface are formed as a consequence of anodic polarization over pitting potentials. In order to reveal the relationship between the pitting locations and microstructure, the metal surfaces were lightly etched by chemicals. The pit-corroding sites of alloy A concentrate on certain weaker spots such as interdendritic arm spacings where compositional segregation occurs. They are fewer in number, but larger and deeper. As the beryllium is added, the pit sites increase in number but the pit size is reduced. All of the pitting sites locate on the interdendritic Ni–Be eutectic phases, showing the lower corrosion resistance of these phases.

5. Concluding remarks

The polarization test results show that the addition of beryllium, even though as low as 0.5 wt %, has a significant effect on lowering the pitting potentials and pitting protection potentials, and on the reduction of passivation ranges for both Ni–15Cr-based and NP2-based alloys in Ringer's solution. This effect is more pronounced for NP2-based alloys, and is attributed mainly to the compositional difference between these two types of alloys.

Measured a.c. impedance spectroscopy shows a significant extent of the reduction of passive-film resistances and an increase of passive-film capacitances as a result of beryllium addition for both types of alloys. This implies that the presence of beryllium in the Ni–Cr alloys could greatly reduce the corrosion resistance and make the passive-film thickening process more difficult.

The volume fraction of Ni–Be eutectic phase increases with increasing beryllium addition. The corroded surface morphology shows that this Ni–Be eutectic phase is less corrosion resistant and suffers from preferential attack.

As a whole, experimental results demonstrate strongly that the addition of beryllium would reduce the corrosion resistance of Ni–Cr dental alloys, as the passive film on the metal surface has been greatly modified. The extent of reduction of corosion resistance is more pronounced for NP2-based alloys.

References

1. G. R. BARAN, *J. Prosthetic Dent.* **50** (1983) 639.
2. American Society for Metals, "Metals Handbook", Vol. 8: "Metallography, Structures and Phase Diagrams" (ASM, Metals Park, Ohio, 1973).
3. R. P. WHITLOCK, R. W. HINMAN, G. T. EDEN, J. A. TESK, G. DICKSON and E. E. PARRY, *J. Dent. Res.* **60** (Special Issue A) (1981) Abstr. 374, 404.
4. E. J. SUTOW, D. W. JONES, R. A. BANNERMAN, D. I. LLOYD and D. HAAS,. *ibid* **60** (Secial Issue A) (1981). Abstr. 376, 404.
5. J. H. C. LIN, R. DUDEK and E. H. GREENER, *ibid.* **64** (1985) Abstr. 1284, 317.
6. J. M. MEYER, *Corros. Sci.* **17** (1977) 971.
7. F. MANSFELD, *Corrosion* **36** (1981) 301.
8. D. D. MACDONALD and M. C. McKUBRE, in "Modern Aspects of Electrochemistry", edited by J. O.' M. - Bockris, B. E. Conway and R. E. White, Vol. 14 (Plenum Press, New York, 1982).
9. D. E. WILLIAMS and J. ASHER, *Corros. Sci.* **24** (1984) 185.
10. D. C. SILVERMAN and J. E. CARRICO, *Corrosion* **44** (1988) 280.
11. T. P. CHENG, W. T. TSAI and J. T. LEE, *J. Mater. Sci.* in press.
12. M. W. KENDIG, E. M. MEYER, G. LINDBERG and F. MANSFIELD, *Corros. Sci.* **23** (1983) 1007.
13. M. M. HEFNEY, A. A. MAZHAR and M. S. EL-BASIOUNY, *Brit. Corros. J.* **17** (1982) 38.

Received 10 July
and accepted 8 November 1989